Proton capture to bound and unbound states of ^{12}C

H. R. Weller, H. Hasan,* S. Manglos, G. Mitev, and N. R. Roberson
Physics Department, Duke University, Durham, North Carolina 27706
and Triangle Universities Nuclear Laboratory, Duke Station, Durham, North Carolina 27706

S. L. Blatt, H. J. Hausman, R. G. Seyler, R. N. Boyd, and T. R. Donoghue
Physics Department, The Ohio State University, Columbus, Ohio 43210

M. A. Kovash
Physics Department, Massachusetts Institute of Technology, Cambridge, Massachusetts 02139

A. D. Bacher and C. C. Foster
Physics Department, Indiana University, Bloomington, Indiana 47401
(Received 7 January 1982)

The cross section for the $^{11}B(p,\gamma)^{12}C$ reaction leading to the 19 MeV region of ^{12}C has been measured at $\theta_{lab}=60°$ for E_p of 23 to 60 MeV. Angular distributions of cross sections and analyzing powers were measured at $E_p=28.7$ MeV. The $^{11}B(p,\gamma_{0,1})^{12}C$ cross sections were measured at $\theta_{lab}=60°$ for E_p of 8 to 60 MeV, with angular distribution measurements at E_p of 14.5, 17.0, and 28.7 MeV. The results are compared to direct capture calculations which, in the case of transitions to the 19 MeV region, treat the final state as both a bound and unbound state. The procedures for calculating direct capture to unbound final states are described. The possible existence of a giant resonance state is discussed.

[NUCLEAR REACTIONS $^{11}B(p,\gamma)^{12}C$; measured $\sigma(E)$ for transitions to the 19 MeV region of ^{12}C at $\theta=60°$ for E_p of 23 to 60 MeV, measured $\sigma(\theta)$ and $A(\theta)$ at 28.7 MeV for these transitions. $^{11}B(p,\gamma_{0,1})^{12}C$, measured $\sigma(60°)$ for E_p of 8 to 60 MeV, $\sigma(\theta)$ at 14.5, 17.0, and 28.7 MeV. Results are compared to direct capture calculations treating the final state both as bound and unbound. Procedures for calculating direct capture to unbound final states are described. The possible existence of giant resonance states is discussed.]

I. INTRODUCTION

Radiative capture reactions at "low" energies have been a valuable probe of nuclear structure for some time. In recent years, much has been learned about the giant resonances built on the ground states of nuclei.[1] The rather large spacing of low-lying states in most of the light nuclei has made it possible to observe γ transitions to these states in addition to the ground state. The simple picture of a giant dipole resonance built upon excited states seems to be able to qualitatively account for many of the observed results. For example, in ^{8}Be and ^{12}C the giant resonances built on the first excited states as observed with the (p,γ_1) reaction are shifted up in excitation energy with respect to the giant resonances built on the ground states. The magnitude of this shift is more or less equal to the spacing between the ground state and the first excited state in ^{8}Be and ^{12}C, respectively.[2]

Little is known about the giant resonances which could, in principle, be built on more highly excited states. However, recent experimental results[3] have shown that transitions to the final states in the region of 19 MeV in ^{12}C could be observed with the $^{11}B(p,\gamma)^{12}C$ reaction. This affords us an opportunity to study the question of the nature of giant resonances built on a rather highly excited state.

What can we expect to observe when looking at electromagnetic strength built on a highly excited state? First of all, the total strength should be governed by the sum rules. The classical dipole sum rule[4] should give us the order of magnitude of $E1$ transition strength to be expected. However, it is worth noting that for excited states the energy-weighted sum rule will be the difference between

the electric dipole absorption strength going up from the state and the decay strength coming down to lower lying levels. This means that a state which has a large amount of the sum rule exhausted in $E1$ transitions to lower lying levels could have as much as two sum rules in the detailed balanced capture strength leading to this state. Of course, only a fraction of this sum rule will normally be found in any one channel.

As far as how this sum rule strength is distributed, we again have little to go on. It is thought that the width of the ground state giant resonances in light nuclei is due mainly to direct escape, while in heavy nuclei it is due to spreading as a result of coupling to higher order particle-hole states.[5] The increased penetrabilities should increase the escape widths as the energy increases. But the escape width may or may not dominate at high energies in light nuclei. Since no detailed calculations have been reported to date, however, we have no quantitative guide as to what width we should expect these "giant resonances" built on highly excited states to have, except that their widths should be significantly greater than the ground state widths.

Previous authors have considered the nature of the strength seen in the $^{11}B(p,\gamma_{19})^{12}C$ reaction. Arnold[6] was the first to elaborate on the suggestion[3] that the observed strength leading to the 19 MeV region of ^{12}C might be the result of direct capture leading to particle-hole states in the residual nucleus, especially the $(d_{5/2}p_{3/2}^{-1})$ configuration. Tsai and Londergan[7] later performed a direct-capture calculation using real potentials, including the effects of residual two-nucleon interactions. The unbound nature of the final state was not taken into account. These authors found a large contribution from such a mechanism for bombarding energies above 40 MeV.

Following this, Halderson and Philpott[8] performed a calculation which treated the final state as an unbound state. They calculated the bremsstrahlung emitted by a proton undergoing a continuum-to-continuum transition while interacting with the target nucleus via a phenomenological optical model potential. They concluded that this single-particle mechanism could account for the major features of the 40–100 MeV data.

It is this latter approach which we shall employ in the present work. Particular attention will be given to the effects of treating the final state as unbound rather than bound. The experimental situation has also evolved since the above mentioned calculations were performed. Information regarding the final states, as well as the energy dependence of the $^{11}B(p,\gamma_{19})^{12}C$ cross section below 40 MeV, have been reported in preliminary form by Blatt *et al.*[9] Details of this work, an Ohio State-Indiana University collaborative effort, along with complementary measurements obtained at Triangle Universities Nuclear Laboratory (TUNL), are given in the present paper. With this larger data base, a more detailed comparison can be made with the predictions of direct capture calculations.

II. EXPERIMENTAL DETAILS

The $^{11}B(p,\gamma)^{12}C$ data of the present work were obtained at the Indiana University Cyclotron Facility (IUCF) utilizing the Ohio State University (OSU) large-crystal γ-ray detection system (OSU/IUCF) and at the Triangle Universities Nuclear Laboratory (TUNL) by the TUNL group. The two experiments were quite similar in all procedures. However, those places where the methods differed will be indicated for completeness.

Excitation functions and angular distributions of cross sections and analyzing powers were determined from γ-ray spectra measured with large NaI(Tl) detectors surrounded by plastic scintillator anticoincidence shields. While differing in detail, these systems follow the basic design philosophy developed at Stanford, Ohio State, and Stony Brook.[10] The TUNL system is based on a 25.4×25.4 cm NaI crystal, and the OSU/IUCF system uses a 25.4×28.5 cm crystal. These systems are described in detail elsewhere.[1,11] Electronics for pileup rejection is provided on each system. Additional gain stabilization circuitry was provided for the OSU/IUCF system, but was found to be unnecessary for the TUNL detector. Time of flight was utilized to reduce background from non-target-related events and neutrons interacting in the detectors. A typical spectrum taken with the TUNL detector is shown in Fig. 1. The OSU/IUCF detector produced generally similar spectra with slightly poorer energy resolution. The measurements performed at TUNL consisted of a yield curve at $\theta_{lab}=60°$ for proton energies of 23 to 32 MeV in 0.5 MeV steps, and an unpolarized angular distribution at $E_p=28.7$ MeV with six angles in the range $55°\leq\theta_{lab}\leq155°$. The measurements obtained at IUCF consisted of yield curve data at 60° for E_p of 23.7 to 60 MeV and analyzing power measurements at $E_p=28.7$ MeV over an angular range of 30° to 145°.

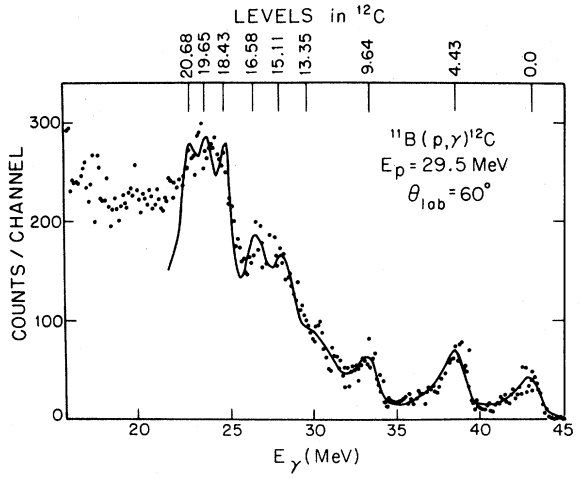

FIG. 1. The $^{11}B(p,\gamma)^{12}C$ spectrum obtained at TUNL. The solid curve is the result of a multiple peak fitting code. The levels in ^{12}C shown are those which were included in the fit.

The spectra obtained at TUNL were fitted by means of a multiple peak fitting computer code. The standard line shape had been previously obtained by using the $^3H(p,\gamma)^4He$ reaction at $E_p = 7$ MeV with the detector setup under identical operating conditions.[12] The OSU/IUCF detector response was determined from spectra taken with the $^3H(p,\gamma)^4He$ reaction along with spectra obtained using monoenergetic γ-ray beams for similar crystals at other laboratories.[13] In addition to the peak corresponding to ground state transitions, peaks having centroids corresponding to transitions to states at 4.43, 9.64, 13.35, 15.11, 16.58, 18.43, 19.65, and 20.68 MeV were included in the fits to the $^{11}B(p,\gamma)$ spectra.[14] The three peaks corresponding to states at 18.43, 19.65, and 20.68 MeV were used to obtain the strength hereafter referred to as the γ_{19} strength. These three peak energies were chosen empirically to best represent the strength seen in this region of the spectra. The solid curve of Fig. 1 shows the result of a typical best fit to one of our spectra.

The absolute cross sections of this work were obtained following the method developed at TUNL.[12] Our efficiency for 15 MeV gamma rays is obtained by normalizing to the $^{12}C(p,\gamma_0)^{13}N$ reaction at the 15.07 MeV (Ref. 15) resonance in ^{13}N. Measurements of the energy dependence of the fraction of the pulses which are rejected by the anticoincidence shield and of the attenuation of the shielding in front of the NaI detector allow us to extrapolate this efficiency to other energies.[12] We estimate an uncertainty of about $\pm 10\%$ in the detector efficiencies determined in this manner. The thick ^{11}B targets used in the TUNL work were prepared by pressing 99% enriched ^{11}B powder into the form of a thin disc. These targets were measured to be 11.9 mg/cm^2 thick with an uncertainty of $\pm 10\%$. This number is based on a comparison to a thin ^{11}B foil target whose thickness was determined [via α-particle (^{241}Am) energy loss, Rutherford scattering, and normalization to previous $^{11}B(p,p)$ data[16]] to be 480 ± 40 μg/cm^2. The normalization between the thick and the thin target was based both on the γ-ray yields using the two targets and the elastic proton yields obtained with a solid-state detector mounted in the scattering chamber. This same solid state detector was used as a monitor for the angular distribution measurements. The targets at IUCF were prepared in a similar manner, and ranged from 20 to 30 mg/cm^2. Since the TUNL data were directly comparable with previously established absolute measurements using the identical experimental setup, the previously reported OSU/IUCF values were normalized by a factor of 0.87 for best overall agreement. (This factor is within the uncertainty of the assumed line shape.) The overall uncertainty in the absolute cross sections reported here is, as a result of efficiency, target thickness, and spectrum stripping uncertainties, as well as the difference in the results of the two experiments, estimated to be $\pm 20\%$.

The angular distribution measurement at TUNL was performed with the NaI detector system positioned so that the back face of the crystal was 106 cm from the target. The Pb collimator was designed so as to fully illuminate the back face of the detector. Spectra were obtained at six angles between 55° and 155°. The unpolarized data obtained at TUNL were combined with the IUCF analyzing power measurements to produce the product $A(\theta)\sigma(\theta)$. In this case the analyzing power is defined as

$$A(\theta) = \frac{N_+ - N_-}{N_+ + N_-} \times \frac{1}{P} ,$$

where N_+ and N_- are the yields obtained for a spin up and a spin down incident proton beam, respectively. P is the beam polarization which, in the present case, was measured using the quench ratio method.[17] The center-of-mass corrected data were fitted in terms of Legendre and associated Legendre polynomials. These expansions were written as:

$$\sigma(\theta) = A_0 \left[1 + \sum_{k=1}^{n} a_k Q_k P_k(\cos\theta) \right] ,$$

and

$$A(\theta)\sigma(\theta)=A_0\left[\sum_{k=1}^{n} b_k Q_k P_k{}^1(\theta)\right],$$

where the Q_k factors correct for finite geometry effects.[1]

III. CALCULATIONS

In order to provide a basis for examining these data for the presence of collective strength (i.e., giant resonances), we shall compare the data to the predictions of the direct capture model.[18,1] In this model the reaction is viewed as proceeding by a mechanism in which the incoming nucleon undergoes a radiative transition from its scattering state into a single-particle state of the residual nucleus. After reviewing the theory for a bound final state, we give particular attention to the effect of realistically treating the final state as unbound.

The direct-capture cross section for nucleons on spin-zero targets going to a final state of definite l,j is, in the case of electric transitions of multipolarity L, given by

$$\sigma_T^L = 2\pi\epsilon_L{}^2\hbar c\left[\frac{e^2}{\hbar c}\right]\frac{k_\gamma}{E_a k_a}(2j+1)B_L{}^2 \times\sum_{l_a j_a}|T^L_{lj,l_a j_a}|^2, \quad (1)$$

where

$$B_L{}^2=\frac{L+1}{(2L+1)L}\frac{k_\gamma{}^{2L}}{[(2L-1)!!]^2}, \quad (2)$$

and

$$T^L_{l_j,l_a j_a}=i^{l_a-l-L}C(jLj_a,\tfrac{1}{2}0\tfrac{1}{2})\sqrt{C^2S_{lj}}\left\langle u_{lj}(r)\left|\frac{(2L+1)!!}{(L+1)k_\gamma^L}[(L+1)j_L(k_\gamma r)-k_\gamma r j_{L+1}(k_\gamma r)]\right|f_{l_a j_a}(r)\right\rangle. \quad (3)$$

In this expression k_a, k_γ are the wave numbers of the incident particle and the outgoing gamma ray, respectively. The orbital and total angular momenta of the incoming nucleon are labeled l_a and j_a, while E_a is the center of mass energy in the entrance channel. The quantity $j_L(k_\gamma r)$ is the spherical Bessel function, and ϵ_L is the effective charge given by[19]

$$\epsilon_L=\frac{A^L Z_n+(-)^L Z}{(1+A)^L}, \quad (4)$$

with A,Z being the mass and charge numbers of the target and Z_n the charge of the incident nucleon. The radial part of the bound state wave function which appears in Eq. (3) $[u_{lj}(r)]$ was normalized according to

$$\int |u_{lj}(r)|^2 dr=1. \quad (5)$$

C^2S_{lj} is the spectroscopic factor associated with the final state. The function $f_{l_a j_a}(r)$ in Eq. (3) is the radial part of the proton partial wave in the incident state $|\phi_\alpha\rangle$:

$$|\phi_\alpha\rangle=\sum_{\mu_a'}\chi_{\mu_a\mu_a'}|s_a\mu_a'\rangle, \quad (6)$$

with

$$\chi_{\mu_a\mu_a'}=\frac{4\pi}{k_a r}\sum_{\substack{l_a j_a\\ \lambda_a\lambda_a' m_a}} i^{l_a} f_{l_a j_a}(r) Y_{l_a}^{\lambda_a *}(\hat{k}_a) \times C(l_a s_a j_a,\lambda_a\mu_a m_a) \times C(l_a s_a j_a,\lambda_a'\mu_a' m_a) Y_{l_a}^{\lambda_a'}(\hat{r}). \quad (7)$$

These continuum wave functions have "plane wave" normalization. This means that for r greater than the range of the nuclear potential, the function $f_{l_a j_a}(r)$ is given by Eq. (2) of the Appendix.

The form of the electromagnetic operator used in Eq. (3) is not the long-wavelength limit (r^L), but does assume Siegert's theorem[20] since the nuclear current operator has been replaced by the charge density operator in obtaining this result. The implications of this choice for the form of the operator have not been fully investigated in the present work. However, this question has been explored in some detail in a recent publication.[21] In the notation of Ref. 21, our choice of operator corresponds to the first term in their so-called density form of the electric operator. The additional terms in this density form are scaled down by a factor of E_γ/mc^2 ($\sim$0.03 here) relative to the first term.

These additional terms have been ignored in the present work.

If we assume that the direct-capture process depends only on the final state parentage to the target ground state plus a single nucleon so that the matrix elements do not depend on the spin of the target nucleus, then we can write the cross section for the case of a target with spin J_a as

$$\sigma_T^L(\text{target spin } J_a)=\frac{2J_f+1}{(2J_a+1)(2j+1)}\sigma_T^L(\text{target spin } 0,\ \text{residual spin } j)\ , \tag{8}$$

where J_f is the total angular momentum of the final state and j is the total angular momentum of the single particle in the final state.[1]

In the case of $M1$ transitions we can perform a similar direct capture calculation. In this case we must evaluate matrix elements of the form

$$\langle u_{lj}(r)\,|\,O_{M1}\,|\,f_{l_aj_a}(r)\rangle\ , \tag{9}$$

where

$$O_{M1}=\mu_0[g_a\vec{J}_a+\mu\vec{\sigma}+\alpha\vec{L}]\ , \tag{10}$$

with

$$\mu_0=\frac{e\hbar}{2mc}\ ,$$

m being the nucleon mass, μ the magnetic moment of the nucleon, $\vec{\sigma}$ the Pauli spin matrix, g_a the gyromagnetic ratio for the target of spin $\vec{J}_a$, and

$$\alpha=\frac{Z+A^2Z_n}{A(1+A)}\ , \tag{11}$$

where Z, Z_n are the charge numbers of the target and projectile, respectively. $\vec{L}$ is the operator for the relative orbital angular momentum of the projectile and target. The cross section in this case is evaluated to be

$$\sigma_T(M1)=\frac{2J_f+1}{(2J_a+1)(2j+1)}\frac{2\pi}{3}\frac{k_\gamma^3}{E_ak_a}\frac{e^2}{\hbar c}\frac{(\hbar c)^3}{(mc^2)^2}\times(2\mu-\alpha)^2\frac{l_a(l_a+1)}{2l_a+1}\,|\,I(M1)\,|^2\delta_{ll_a}\ , \tag{12}$$

where the radial integral $I(M1)$ is given by

$$I(M1)=\int u_{lj}(r)f_{l_aj_a}(r)\,dr\ . \tag{13}$$

The matrix element of $g_a\vec{J}_a$ vanishes in this direct capture model since the operator contains only the internal coordinates of the core.[22] If different potentials are used to generate the wave functions for the initial and final states, terms which should properly vanish owing to orthogonality may not. We have arbitrarily set such terms ($lj=l_aj_a$) equal to zero in our calculations.

In the preceding discussion we have considered the incident nucleon to be captured into a final state which is bound. We would now like to consider the case in which the nucleon is captured into a final state which is a continuum (resonance) state having an energy E_f and a width Γ. In the direct capture model, the captured nucleon is emitted when this continuum state decays. In this situation the differential cross section for the capture process depends on the energy of the final state. The total cross section for capture to a specific continuum final state is obtained by integrating over the energy of the final (resonance) state. We have

$$\sigma_T^L=\int\int\frac{d^2\sigma(E_f)}{d\Omega\,dE_f}dE_f\,d\Omega\ , \tag{14}$$

where E_f is the energy of the final state and $d\sigma(E_f)/dE_f$ is the differential cross section with respect to E_f. The quantity $d\sigma(E_f)/dE_f$ is, for an electric transition of multipolarity L, a target of spin J_a, and a final state of spin J_f, given by:

$$\frac{d\sigma(E_f)}{dE_f}=\frac{4mc^2}{E_a}\frac{k_\gamma}{k_fk_a}\frac{\epsilon_L{}^2e^2}{(\hbar c)^2}\frac{2J_f+1}{2J_a+1}\times\sum_{l_aj_a}B_L{}^2C^2(jLj_a,\tfrac{1}{2}0\tfrac{1}{2})\,|\,I^L_{lj,l_aj_a}\,|^2\ , \tag{15}$$

where we capture to a state having a single particle with a specific l_j. In this expression k_f is the continuum final state wave number of the captured particle of reduced mass m.

The integral I^L_{lj,l_aj_a} is

$$I^L_{lj,l_aj_a}=\int_0^\infty f_{lj}(r)\left\{\frac{(2L+1)!!}{(L+1)k_\gamma^L}[(L+1)j_L(k_\gamma r)-k_\gamma r j_{L+1}(k_\gamma r)]\right\}f_{l_aj_a}(r)\,dr\ , \tag{16}$$

where the continuum radial wave functions are defined from Eq. (7). The form of the operator used here is identical to that of Eq. (3). The integrals I^L_{lj,l_aj_a} must be evaluated numerically. However, since the integrand oscillates out to infinity it is impractical (in most cases) to integrate directly. In order to avoid this problem we have utilized the method developed by Vincent and Fortune[23] for evaluating similar integrals which appear in stripping reactions when the final state is unbound. In this technique rapid convergence of the integral is obtained by integrating along the imaginary axis. A full discussion of this procedure is given in the Appendix.

After evaluating these integrals for various final proton energies E_f, we must integrate over the final proton energy. If we assume a Breit-Wigner shape for the cross section as a function of E_f, this amounts to multiplying the cross section at the resonance energy by the factor $\pi\Gamma/2$, where Γ is the full-width-at-half-maximum for the resonance in the (p,γ) cross section as a function of E_f. A comparison of this result with exact numerical integrations indicated that this procedure is accurate to better than 95% in the present case.

Angular distribution coefficients were calculated from the relative transition matrix elements of Eq. (3). In the case of the continuum calculations the matrix element in Eq. (3) is replaced by that of Eq. (16). In both cases the normalization condition

$$\sum_{Ll_aj_a} \epsilon_L{}^2 B_L{}^2 \, | \, T^L_{lj,l_aj_a} \, |^2 = 1 \, ,$$

was used to evaluate $\epsilon_L B_L T^L_{lj,l_aj_a}$, the relative transition amplitude for the incident channel l_aj_a going to a specific final state having lj. The relative phases are just those of the T^L_{lj,l_aj_a}'s of Eq. (3). These were used in the standard expression for the angular distribution expansion coefficients (see Ref. 1) to obtain the a_k and b_k coefficients.

IV. RESULTS AND DISCUSSION

In order to discuss the present data for the $^{11}B(p,\gamma_{19})^{12}C$ reaction, especially with regard to the presence or lack of a giant resonance feature, we will first review the cases of $^{11}B(p,\gamma_0)$ and $^{11}B(p,\gamma_1)$ experimentally and compare them to the results of direct capture calculations. In these two cases the existence of a giant resonance state is well established. Therefore, this should provide a reference for a similar comparison in the $^{11}B(p,\gamma_{19})^{12}C$ case and hopefully allow us to make a critical evaluation regarding the possible presence of a giant dipole resonance (GDR) in the (p,γ_{19}) case.

The results of the present measurements of the $^{11}B(p,\gamma_0)$ and $^{11}B(p,\gamma_1)$ cross sections at $\theta_{lab}=60°$ are shown in Fig. 2. The lower energy data were obtained with the TUNL FN tandem, while the 23 to 32 MeV data were obtained with the TUNL cyclograaff. The OSU/IUCF data extend these results to $E_p=60$ MeV. These reactions have been previously measured for proton energies of 4 to 29 MeV (Refs. 2 and 24–28). However, there have been some discrepancies in the values of the abso-

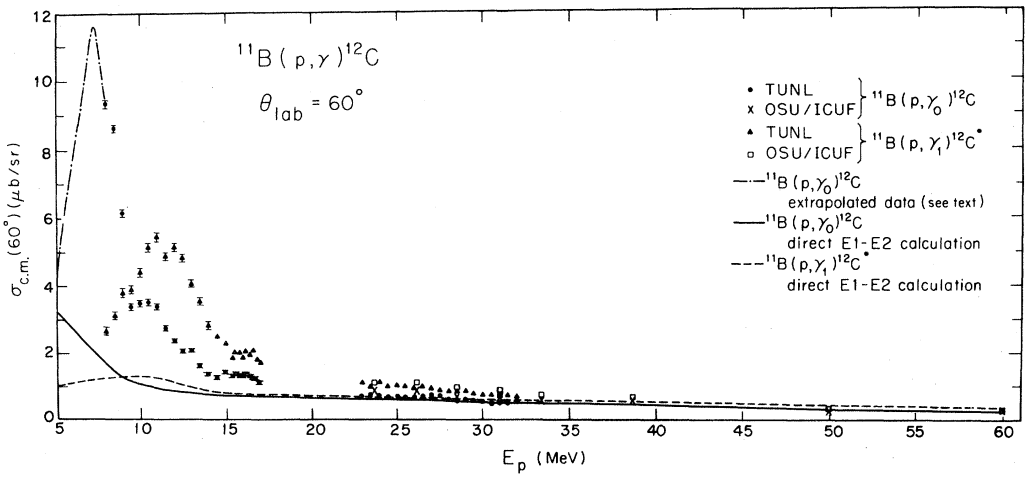

FIG. 2. The TUNL and OSU/IUCF data for the $^{11}B(p,\gamma_0)^{12}C$ and $^{11}B(p,\gamma_1)^{12}C$ cross sections at $\theta_{lab}=60°$. The dotted-dashed line extrapolates the (p,γ_0) data down to $E_p=5$ MeV using the data of Ref. 24. The solid and dashed curves are the results of direct capture calculations for the (p,γ_0) and (p,γ_1) reactions, respectively. The error bars shown represent only the statistical uncertainties.

lute cross sections and in the shape of the yield curve, especially for the $^{11}B(p,\gamma_0)^{12}C$ case. These discrepancies have recently been resolved in a joint TUNL-BNL effort,[29] which showed that a correction factor which varies almost linearly from a value of 0.8 at $E_p=6$ MeV to a value of 0.6 at $E_p=14$ MeV should be applied to the $^{11}B(p,\gamma_0)^{12}C$ cross section data of Ref. 24. The point of Fig. 2, however, is to compare the cross sections for transitions to the ground and first excited states to the predictions of a direct-capture calculation. The solid and dashed curves represent the results of a pure direct $E1+E2$ calculation. The final (bound) states were represented by single particle wave functions obtained by adjusting a Wood-Saxon potential to produce the correct binding energies for the $p_{3/2}$ and $p_{1/2}$ single-particle states. The spectroscopic factors were obtained from the calculations of Cohen and Kurath.[30] The optical model potentials used to produce the incoming distorted waves were those of Watson[31] *et al.* What we observe here is that in the region of the giant dipole resonances for the ground and first excited states of ^{12}C ($E_p\sim7.25$ and ~11.0 MeV, respectively), the direct capture cross section has the wrong energy dependence, and underestimates the experimental cross sections by a factor of about 5. However, as we go to higher energies, this discrepancy disappears. By the time we get to $E_p=30$ MeV we find that the (p,γ_0) cross section is in excellent agreement with the direct-capture prediction while the (p,γ_1) cross section is about 20% higher than the calculation, with the two appearing to converge. At still higher energies, the direct capture calculations continue to give a satisfactory description of the measured cross sections.

The predictions of the direct calculations can also be compared to the measured angular distributions. The experimental angular distributions were expanded in terms of Legendre polynomials as previously discussed. In the present work angular distributions for (p,γ_0) and (p,γ_1) were obtained at $E_p=14.5$, 17.0, and 28.7 MeV. These data allow us to compare the present experiment to previous works. The a_k coefficients of the present work are shown in Fig. 3(a) for the (p,γ_0) case and in Fig. 3(b) for the (p,γ_1) case. The results of previous measurements are also shown here. Note that the data of Allas *et al.*[24] are represented by a dashed line which was drawn through the numerous data points of that experiment. Table I lists the present results.

The solid curves in Figs. 3(a) and 3(b) are the results of the direct $E1+E2$ calculation. The remarkable qualitative agreement with the data is somewhat surprising. It has been previously shown that the GDR does not have a large effect on the a_2 coefficient, the dominant coefficient in determining the shape of the angular distributions at the energies of the GDR. Polarized capture experiments have been important in developing our understanding of this point.[1] The average potential well seems to determine the angular distribution, at least to first

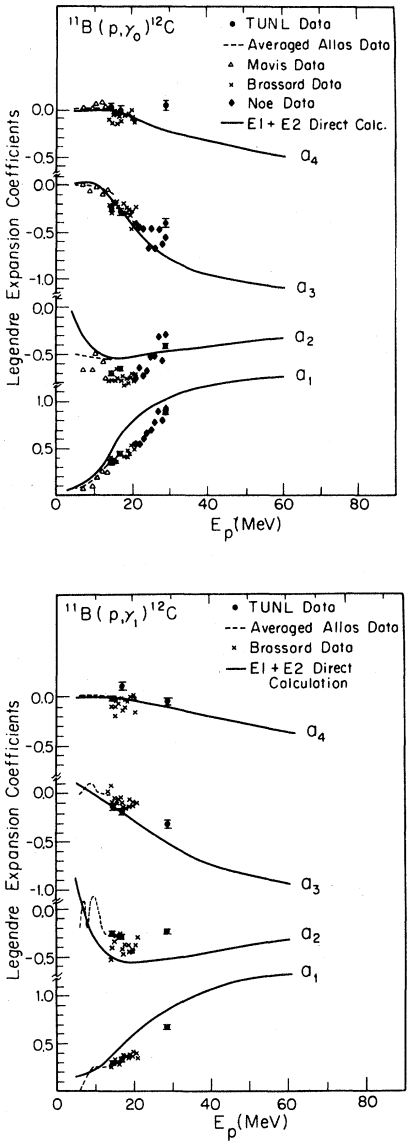

FIG. 3 (a) The experimental a_k coefficients for the $^{11}B(p,\gamma_0)^{12}C$ reaction are shown here along with the predictions of the direct $E1+E2$ capture calculation. TUNL, present work; Allas, Ref. 24; Mavis, Ref. 27; Brassard, Ref. 25; and Noe, Ref. 26. (b) Same as (a) but for $^{11}B(p,\gamma_1)^{12}C$.

TABLE I. Angular distribution coefficients.

		$^{11}B(p,\gamma_0)^{12}C$		
E_p	a_1	a_2	a_3	a_4
14.5	0.345±0.012	−0.702±0.018	−0.251±0.028	0.028±0.031
17.0	0.436±0.014	−0.657±0.022	−0.285±0.030	0.005±0.037
28.7	0.881±0.016	−0.408±0.028	−0.376±0.039	0.044±0.039
		$^{11}B(p,\gamma_1)^{12}C$		
E_p	a_1	a_2	a_3	a_4
14.5	0.291±0.009	−0.256±0.014	−0.141±0.019	−0.022±0.023
17.0	0.331±0.011	−0.259±0.017	−0.192±0.022	0.122±0.029
28.7	0.656±0.013	−0.236±0.022	−0.333±0.029	−0.039±0.033

order, and this is relatively stable independent of whether one is on or off of the GDR.[1]

The results for a_1 and a_3 are, however, unexpected, at least at first glance. These coefficients are determined by $E1-E2$ interference terms. Both a_1 and a_3 should be proportional to the square root of the ratio of the $E2$ cross section divided by the $E1$ cross section. The direct capture model makes a definite prediction for this ratio. If the $E1$ strength is enhanced by virtue of a GDR by, say, a factor of 5, with the $E2$ strength following the direct capture value, the effect could be expected to show up in a_1 and a_3 as a factor of ~ 2 departure from the direct model prediction. Thus we see that these coefficients could provide a valuable diagnostic tool in the search for giant resonances since they depend on relative rather than absolute cross sections.

In the case of (p,γ_0) the GDR occurs in the region of $E_p=7$ to 10 MeV. Unfortunately, a_1 and a_3 are so small here that it is almost impossible to claim that an effect is present. The overall level of agreement between theory and experiment is just not good enough to distinguish, say, between an a_1 of 0.05 and 0.10.

In the case of (p,γ_1) the GDR is at a slightly higher energy. Here one might expect to see a deviation from the direct behavior in a_1 and a_3 at and below $E_p=14$ MeV. Again there is no observable effect, i.e., the quality of the agreement between the direct model prediction and the data does not change significantly as we move into the region of the GDR. The accuracy of the model is apparently not sufficient to be able to use it to observe nondirect behavior in the a_k coefficients. Of course the oscillations observed in the (p,γ_1) data, especially in a_2 below 12 MeV, indicate nondirect behavior. But this is more suggestive of intermediate structure or secondary doorways[32] than it is of the existence of the GDR itself. And again, even these effects are not very noticeable in a_1 and a_3. These observations lead us to the following conclusions:

(1) The typical giant resonance (built on the ground state or some other "low lying" state) observed in a proton capture channel gives rise to an enhancement in the absolute cross section of the order of a factor of 5 above the direct capture model prediction. We should expect this factor to decrease as we go to giant resonances built on more highly excited states for two (not independent) reasons: the opening of more channels and the spreading out of the GDR. Of course, detailed nuclear structure effects could also influence this result significantly.

(2) In the case of $^{11}B(p,\gamma_0)$ and $^{11}B(p,\gamma_1)$ the GDR is well established and clearly observed in the proton capture reaction. However, it is difficult to observe its presence in the angular distribution coefficients, for two reasons: First, the low proton energies involved lead to small a_1 and a_3 coefficients, presumably as a result of the small direct $E2$ strengths present at these energies. Therefore, changes in these coefficients are difficult to observe. Second, the overall quality of the agreement between the direct calculation and the a_k coefficients is reasonably good, but not good enough to see the effects expected from the presence of the GDR. In the case of γ_{19} we might, however, expect to be in a more favorable situation regarding the sensitivity of the a_1 and a_3 coefficients, since the background values (i.e., the pure direct capture predictions) will be considerably larger. But we must be careful in drawing conclusions since there are some obvious complicating factors. First, the $E2$ strength could deviate (in all cases being described) from the direct prediction and reduce the effect of any enhance-

ment of the $E1$ term. Furthermore, a_1 and a_3 are actually sums of many interference terms which contain differences between the phases of the relevant transition amplitudes. Although polarized capture data have indicated that these phases vary slowly and smoothly across the giant resonances and are not very sensitive to the presence of the resonances,[1] it is possible for small phase changes to produce large effects in the observed a_k coefficients.

Based on the above considerations we can see that our strongest tool for establishing the existence of a giant resonance is the behavior of the cross section as a function of energy. If this is not a convincing test due, for example, to a broadened GDR as well as competition with an energy dependent direct capture strength, we can investigate the absolute cross section. However, since this is the most troublesome aspect of most experiments and theories, we can expect difficulty here. Our second set of observables is the angular distribution coefficients (the a_k) which are independent of the absolute cross sections. Unfortunately, as just discussed, there is apparently no unambiguous way to interpret these *vis a vis* the presence of a giant resonance.

The results of the measurements of the 60° yield curve for the ^{11}B$(p,\gamma_{19})^{12}$C reaction are shown in Fig. 4. Both the TUNL and the OSU/IUCF data are shown here. Although a few of the data points in the 23–32 MeV region deviate from a smooth behavior, these fluctuations are relatively minor and can be attributed to spectrum stripping and background problems. Hence we conclude that there is no convincing evidence in these data for any significant fine or intermediate structure at these excitation energies. As previously discussed, an overall uncertainty of ±20% should be associated with the absolute cross sections shown here.

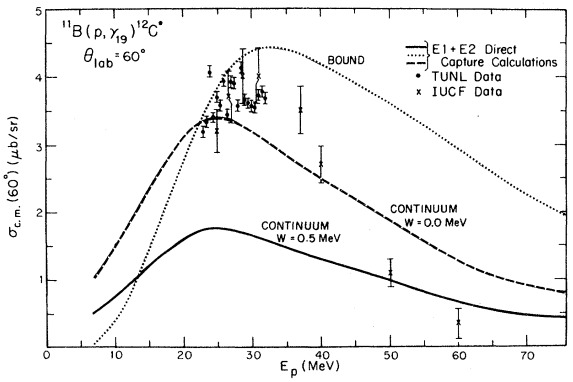

FIG. 4. The ^{11}B$(p,\gamma_{19})^{12}$C* center-of-mass cross section as a function of incident proton energy at $\theta_{lab}=60°$. Both TUNL and OSU/IUCF data are shown. The error bars on the TUNL data are statistical only. Those on the OSU/IUCF data include the estimated error due to target thickness and stripping uncertainties. The overall error on the absolute cross section shown here is estimated as ±20%. The solid curves represent the three direct capture calculations [bound final state, continuum final state ($W=0.0$), continuum final state ($W=0.5$ MeV)]. As discussed in the text, the continuum final state ($W=0.5$ MeV) calculation should be the most realistic.

Since the present NaI detectors cannot resolve the individual final states in the 19 MeV region, we cannot specify exactly which levels are being populated here. The three lines needed to fit the spectra suggest that we are seeing strength to the 3^- and 4^- levels in this region,[14] but the presence of additional strength cannot be ruled out. It is interesting to note here that the spins and parities of the low lying levels of ^{12}C indicate that if the 4^- states dominate the 19 MeV region, there should be little downward $E1$ strength, and therefore no more than one $E1$ sum above the 19 MeV states. Investigations of possible background contaminations were undertaken in our spectrum fitting procedures. We could not generate any fits nearly as consistent (i.e., having good χ^2) if a background as large as 10% of the peak sum was included. We therefore conclude that the strength which we have extracted corresponds to capture strength to the levels in ^{12}C between 18 and 21 MeV. If there is any background (owing to pileup, contaminants, other reactions, etc.) present in our spectra, it appears to be less than a 10% effect.

The first calculation which we attempted was a direct $E1+E2$ capture calculation in which the final state(s) at 19 MeV was treated as a bound $d_{5/2}$ single particle state. Previous particle-hole calculations[7,33] and shell model calculations[8] have indicated that one should expect the $(d_{5/2},p_{3/2}{}^{-1})$ strength to be concentrated near 19 MeV in ^{12}C. Both the $2s_{1/2}$ and $1d_{3/2}$ single particle strength would be expected to be located 3–5 MeV from the $d_{5/2}$ strength.[8] We therefore assume that the $d_{5/2}$ single particle strength is the dominant single particle strength in the (p,γ_{19}) reaction. A Woods-Saxon potential was found which placed the $d_{5/2}$ single-particle state just below the proton threshold. In fact, the calculation was found to be rather insensitive to the binding energy used; it was varied from −0.1 to −5.0 MeV. The calculation shown in Fig. 3 placed the $d_{5/2}$ single particle state at 15 MeV (a binding energy of −1.0 MeV). Although the energy of the state used to generate the single particle

wave function in the radial matrix element was not the physical energy, the energy in the kinematic factors which appear in the cross section expression [see Eqs. (1)–(3)] was taken to be 19.2 MeV. The parameters of the Woods-Saxon potential which generated this $d_{5/2}$ state were $V=63.3$ MeV, $r_0=1.25$ fm, $a=0.65$ fm, and $V_{so}=8.75$ MeV.

The continuum wave function was generated by using the optical model potential found by fitting 30 MeV proton elastic scattering data.[34] In order to keep the calculation as transparent as possible, no energy dependence was given to these potential parameters. The spectroscopic factor (C^2S) was set equal to 1.0. The results of this "bound state" calculation for $E1+E2$ radiation are shown in Fig. 4.

The above calculation indicates that the cross section is dominated by $E1$ capture from the $f_{7/2}$ channel. At 25 MeV, for example, this term accounts for 81% of the cross section. Furthermore, the $E2$ cross section is relatively unimportant, accounting for about 6% of the total cross section at 29 MeV. If the $M1$ cross section is computed according to Eq. (12), with the $d_{5/2}\rightarrow d_{5/2}$ strength set equal to zero, it accounts for $\sim 3\%$ of the cross section at 29 MeV. As discussed in Sec. III, this calculation is not very reliable owing to orthogonality problems. Because of this, plus the fact that it has a negligible effect on the cross section and a relatively small effect on the angular distribution coefficients (see below), it is not included in the calculation presented in Fig. 4.

The results of the polarized and unpolarized measurements of the $^{11}B(p,\gamma_{19})^{12}C$ angular distribution at 28.7 MeV are shown in Fig. 5. The solid curves are the results of Legendre and associated Legendre polynomial fits to the data. It was found that satisfactory fits were obtained when fitting through third order polynomials in both cases. The resulting a_k and b_k coefficients, which have been corrected for (minor) finite geometry effects, are presented in Table II. Angular distribution coefficients were calculated with the bound state direct capture model discussed above. The results are presented in Table II along with the experimental values. It can be seen here that this rather simple model of direct $E1+E2$ capture gives a good description of the angular distribution data, the exception being the b_1 coefficient.

On the basis of this result it appears as though the direct capture model can account for the main features of the (p,γ_{19}) reaction. Both the peaking near 30 MeV and the angular distribution results can be obtained from this model. However, the en-

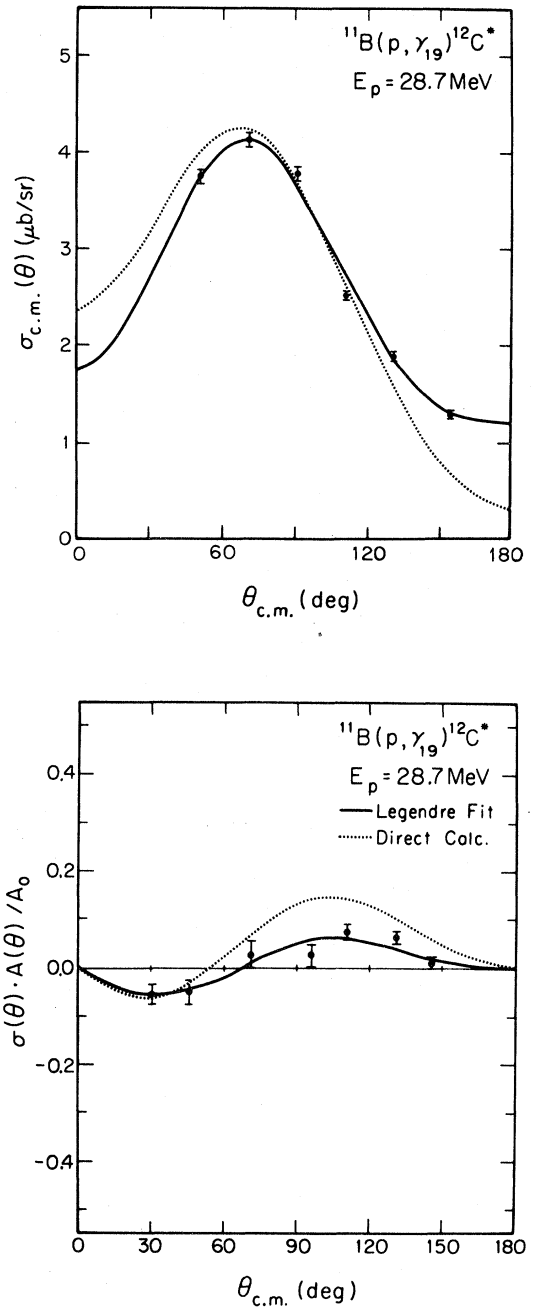

FIG. 5. The angular distribution of the cross section and of the product of the cross section times the analyzing power for the $^{11}B(p,\gamma_{19})^{12}C$ reaction at $E_p=28.7$ MeV. The error bars represent the statistical uncertainties associated with the data points. The solid curves are the result of Legendre and associated Legendre polynomial fits to the data. The dashed curves are the results of the direct capture calculation (continuum final state, $W=0.5$ MeV) as described in the text. The cross section calculation was normalized by a factor of 2.5 for the purpose of comparing to the data.

TABLE II. Angular distribution coefficients.

	^{11}B$(p,\gamma_{19})^{12}$C $E_p=28.7$ MeV		
Experiment	Bound calc	Continuum calc $W=0$	Continuum calc $W=0.5$
$a_1=$ 0.37±0.05	0.44	0.56	0.55
$a_2=-0.50\pm0.09$	−0.57	−0.52	−0.52
$a_3=-0.27\pm0.07$	−0.16	−0.22	−0.20
$b_1=$ 0.02±.016	0.084	0.092	0.096
$b_2=-0.027\pm.008$	−0.044	−0.041	−0.040
$b_3=-0.016\pm.006$	−0.022	−0.026	−0.027

ergy dependence of the data above 30 MeV is not reproduced by the calculation. Furthermore, the assumption of a pure $d_{5/2}$ single particle state ($C^2S=1$) at 19 MeV is most certainly unrealistic. In addition, no attempt was made to take account of the energy dependence of the optical model parameters in this result. And finally, the treatment of the final state as a bound state is certainly wrong.

An investigation of the optical model potential used to generate the incident wave functions was performed in order to understand the peaking observed in the (p,γ_{19}) calculation. It was found that this peak position could be moved significantly by altering the incident potential. For example, the peak occurs at around $E_p=18$ MeV if the potential used to generate the final $d_{5/2}$ single particle state is also used for the incident protons. An examination of the complex phase shift associated with the $f_{7/2}$ partial wave for the potential of Ref. 34 indicates, as shown in Fig. 6, that this peaking is associated with a minimum in the inelastic parameter η, where $\eta=e^{-2\gamma}$ and γ is the imaginary part of the phase shift associated with the $f_{7/2}$ partial wave. The real part of the phase shift δ is also shown here. These results imply a maximum in the reaction cross section near 27 MeV, and a resonancelike behavior in the $f_{7/2}$ elastic channel, albeit with a real potential not strong enough to produce a 90° resonance phase shift. We also investigated the effects of energy dependence of the optical model potential used to generate the incident wave function by using potentials found for ^{12}C+p at 30.4, 40, 61, and 100 MeV. These calculations indicated that no reasonable energy dependence would give an effect which would bring the results of the present calculation significantly closer to the data.

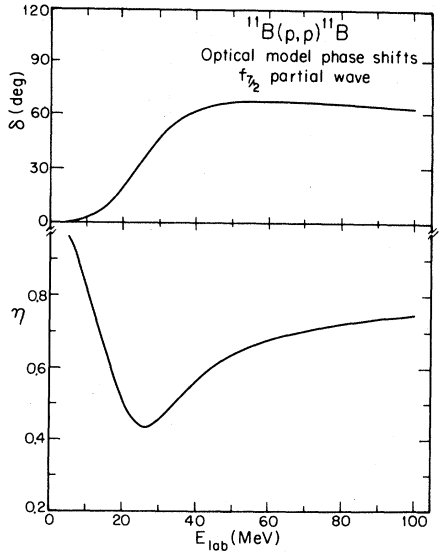

FIG. 6. The real part of the phase shift and the inelastic parameter ($\eta=e^{-2\gamma}$) associated with the $f_{7/2}$ partial wave for the potential (Ref. 34) used to describe the incident channel in the direct capture calculations.

In order to pursue the direct capture model further we performed a calculation in which the final state was treated as a continuum state. The expressions and integration techniques used were given in Sec. III. The final state was described by an optical potential which initially had the imaginary part set equal to zero. The potential parameters of Table III placed a $d_{5/2}$ resonance at $E_p=3.5$ MeV ($E_x=19.17$ MeV). The potential of Ref. 34 was again used to generate the incident wave function. After performing the necessary integrals, including an integration over the final state energies, this direct $E1+E2$ capture model gave the 60° yield curve shown in Fig. 4 and the angular distribution

TABLE III. Optical model parameters (energies are in MeV, geometrical parameters in fm).

Incident potential	Final state potential
$V=45.2$	$V=55.0$
$W=$ 3.38	$W=$ 0.0, 0.5
$V_{so}=7.79$	$V_{so}=6.64$
$r_0=$ 1.09	$r_0=$ 1.23
$r_s=$ 1.3	$r_s=$ 1.16
$r_{so}=0.98$	$r_{so}=1.03$
$a_0=$ 0.59	$a_0=$ 0.66
$a_s=$ 1.01	$a_s=$ 0.83
$a_{so}=0.57$	$a_{so}=0.66$
$r_c=$ 1.29	$r_c=$ 1.10

coefficients of Table II. The results of a second continuum calculation, which added an imaginary potential of 0.5 MeV to the final state potential, are also shown in Figs. 4 and 5 and Table II. Although this value of W was chosen somewhat arbitrarily,[31] an effort was made to keep the width of the resonance in the vicinity of 0.5 MeV. The addition of this term should give a more realistic representation of the final state. A detailed comparison with the available elastic proton scattering data[35] in the energy region of E_p from 3 to 4 MeV indicates that the real situation is considerably more complicated than this model since fragmentation of this state as well as other states are almost certainly present in these data.

Of the three curves shown in Fig. 4, the continuum calculation with $W=0.5$ MeV should be the most realistic. This calculation peaks 3 to 4 MeV below the apparent peak in the data. It also fails to have the correct energy dependence, falling off much too slowly as the energy increases. Furthermore, since the full $d_{5/2}$ spectroscopic strength is included in these calculations, all of these calculations must be regarded as upper limits for the predictions of the model. As seen in Table II, the model of $E1$-plus-$E2$ direct capture gives good agreement with the angular distribution data, especially for a_2 and a_3, b_2 and b_3. Although the addition of direct $M1$ can lower a_1 by 0.05 and b_1 by 0.025, these small $M1$ effects in a_1 and b_1 are not significant enough to be useful.

The present direct calculations seem unable to account for all of the cross section observed as a function of energy in the $^{11}\mathrm{B}(p,\gamma_{19})^{12}\mathrm{C}$ reaction when realistic potentials and spectroscopic factors are assumed. As shown in Fig. 5 and Table II, the $E1$-plus-$E2$ direct capture model does a reasonable job of predicting most of the angular distribution results, although the predicted analyzing powers are about a factor of 2 larger than the measured values at back angles. We therefore conclude that it is likely that there is additional strength present in the data, but at present we are unable to specify its nature; a giant resonance kind of effect, in this case enhanced above the direct capture by a factor of about 3, is one possibility.

Londergan and Ludeking[36] have shown that the addition of a resonance at $E_x=42$ MeV with a width of ~ 12 MeV can greatly improve the agreement between their direct capture calculation and the data of the present experiment. However, since our direct capture calculation peaks so much closer to the peak in the data (theirs peaks near 21 MeV), and since the expected width of this resonance is rather uncertain, such an addition was not performed here. It is unfortunate that in this reaction the peak in the direct capture cross section lies so close to where one might expect a peak due to a giant resonance built on the 19 MeV state(s). Perhaps further studies in which this is not the case[37] will help us to determine whether or not giant resonances built on such highly excited states are unambiguously perceptible in proton capture reactions.

We are grateful to J. M. Lafferty, Jr. and S. R. Cotanch for their help in performing these calculations.

APPENDIX

The integrals I^L_{lj,l_aj_a} of Eq. (16) were evaluated numerically. Since the integrand oscillates out to infinity, it is impractical to integrate directly. The integration can, however, be performed economically by employing the method developed by Vincent and Fortune[23] for evaluating similar integrals which appear in calculations involving stripping reactions leading to unbound final states. In their procedure, rapid convergence of the integral is achieved by exploiting the fact that the Coulomb wave functions decay rapidly along the imaginary axis in the complex r plane.

In this method the integral I^L_{lj,l_aj_a} is first broken up into two parts:

$$I^L_{lj,l_aj_a}=\int_0^{R_{\max}} f_{lj}(r)O_{EL}(r)f_{l_aj_a}(r)\,dr + \int_{R_{\max}}^{\infty} f^c_{lj}(r)O_{EL}(r)f^c_{l_aj_a}(r)\,dr\ , \tag{A1}$$

where the functions $f(r)$ and the electric multiple operator are as defined in Sec. III. The wave functions for $f^c_{lj(l_aj_a)}$ for $r>R_{\max}$ are purely Coulombic. The distance $R_{\max}$ is chosen along the real axis such that the effect of the nuclear potential is zero for $r>R_{\max}$. The wave functions $f^c_{lj}(r)$ can be written as

$$f^c_l(r)\sim\frac{i}{2}[H_l^-(kr)-\eta_l H_l^+(kr)]e^{i\sigma_l}\ , \tag{A2}$$

where

$$H_l^{\pm}=G_l\pm iF_l,\ \text{and } F_l \text{ and } G_l$$

are the regular and irregular Coulomb functions, σ_l is the Coulomb phase shift, and η_l is the nuclear scattering amplitude (note: the unnecessary subscripts on f^c have been dropped for simplicity).

The first integral in Eq. (A1) was evaluated by direct numerical integration, with $R_{\max}$ taken to be 30 fm. The second integral was evaluated by first noting that the asymptotic form of the Coulomb functions $H_l^{\pm}$ is given by

$$H_l^{\pm} \underset{r\to\infty}{\to} (f \pm ig)e^{\pm i\theta_l} , \tag{A3}$$

where

$$\theta_l = kr - \frac{Z_1 Z_2 e^2}{\hbar v}\ln(2kr) - \frac{l\pi}{2} + \sigma_l . \tag{A4}$$

The functions f and g are rapidly converging series which are readily calculated. If we now go to the complex r plane, we find that H_l^+ decays exponentially in the upper half-plane, and H_l^- has a similar behavior in the lower half-plane. This property of the Coulomb functions makes the evaluation of the integral straightforward. Substituting Eq. (A2) into the second integral of Eq. (A1) gives:

$$\int_{R_{\max}}^{\infty} f_{ij}^{c}(r) O_{EL}(r) f_{l_a j_a}^{c}(r)\, dr = I_1 + I_2 , \tag{A5}$$

where

$$I_1 = \tfrac{1}{4}\eta_{l_a} e^{i(\sigma_{l_a}+\sigma_l)} \int_{R_{\max}}^{\infty} H_{l_a}^{+}(k_a r) O_{EL}(r)[H_l^{-}(kr) - \eta_l H_l^{+}(kr)]dr , \tag{A6a}$$

and

$$I_2 = -\tfrac{1}{4} e^{i(\sigma_{l_a}+\sigma_l)} \int_{R_{\max}}^{\infty} H_{l_a}^{-}(k_a r) O_{EL}(r)[H_l^{-}(kr) - \eta_l H_l^{+}(kr)]dr . \tag{A6b}$$

The integral I_1 was evaluated by going into the upper half of the complex r plane and integrating along the contour as shown in Fig. 7. So

$$I_1 = \lim_{y_{\max}\to\infty} \left\{ \frac{i}{4}\eta_{l_a} e^{i(\sigma_{l_a}+\sigma_l)} \int_{y=0}^{y=y_{\max}} H_{l_a}^{+}(k_a r_+) O_{EL}(r_+)[H_l^{-}(kr_+) - \eta_l H_l^{+}(kr_+)]dy + \int_{C^+}\{\ \} \right\} , \tag{A7}$$

where r_+ is equal to $R_{\max}+iy$. Since the integrand vanishes at infinity on the arc of the circle, the last term, the integral along C^+, vanishes. The remaining integral along y in Eq. (A7) can be evaluated numerically. We found that convergence was obtained with $y_{\max}=50$ fm. The integral I_2 was evaluated by a similar procedure applied to the lower half of the complex r plane.

The Coulomb functions $H_l^{\pm}(kr)$ were obtained in the complex r plane by solving the Coulomb equation with r complex using the Fox-Goodwin method[38,39] modified for a complex integration variable. If $H_l(r_0)$, $H_l(r_1)$ are values of H_l at two points r_0 and $r_1 = r_0 + h$, then the value of $H_l(r_2)$ at $r_2 = r_1 + h$ is given by

$$\left[1 - \frac{h^2}{12}t_2\right] H_l(r_2) = (2 + \tfrac{5}{6}h^2 t_1) H_l(r_1) - (1 - \tfrac{1}{12}h^2 t_0) H_l(r_0) , \tag{A8}$$

where, with $\rho_m = kr_m$,

$$t_m = -1 + \frac{2\eta}{\rho_m} + \frac{l(l+1)}{\rho_m^2} .$$

In the case of r being complex, h is also complex. Since we integrate only along the y axis, we have $h = i\,|h|$, where $|h|$ is the step size along the y axis. Taking $r_0 = R_{\max} \pm iy_{\max}$ such that the $H_l^{\pm}$ have their asymptotic forms [Eqs. (A3) and (A4)] allows us to use Eq. (A8) to compute $H_l^{\pm}$ elsewhere. The value of $y_{\max}$ was taken such that $ky_{\max} \sim 10$. Once the values of $H_l^{\pm}$ were found, the integration of Eq. (A7) was performed using Simpson's rule.

One means of verifying the validity of this calculation is to investigate the behavior as the continuum state was lowered in energy and to compare the results to the bound final state treatment as the energy of the bound state was raised. It was found that excellent agreement between the two calculations could be obtained as the energies approached each other.

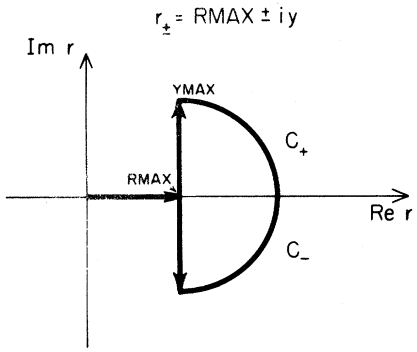

FIG. 7. The integration path shown in the complex r plane used to evaluate the integrals I_1 (upper half of the plane) and I_2 (lower half of the plane).

*Permanent address: Physics Department, University of Poona, Pune, India.

[1]H. R. Weller and N. R. Roberson, Rev. Mod. Phys. 52, 699 (1980).

[2]M. Suffert, in *Proceedings of International Conference on Photonuclear Reactions and Applications,* edited by Barry Berman (AEC, Oak Ridge, Tennessee, 1973), p. 741.

[3]M. A. Kovash, S. L. Blatt, R. N. Boyd, T. R. Donoghue, H. J. Hausman, and A. D. Bacher, Phys. Rev. Lett. 42, 700 (1979).

[4]O. Nathan and S. G. Nilsson, in *Alpha-, Beta-, and Gamma-ray Spectroscopy,* edited by K. Siegbahn (North-Holland, Amsterdam, 1965), Chap. X.

[5]Michael Danos and Walter Greiner, Phys. Rev. 138, 876 (1965).

[6]L. G. Arnold, Phys. Rev. Lett. 42, 1253 (1979).

[7]T. Tsai and J. T. Londergan, Phys. Rev. Lett. 43, 576 (1979).

[8]Dean Halderson and R. J. Philpott, Phys. Rev. Lett. 46, 100 (1981).

[9]S. L. Blatt, M. A. Kovash, T. R. Donoghue, R. N. Boyd, H. J. Hausman, and A. D. Bacher, Bull. Am. Phys. Soc. 24, 843 (1979); S. L. Blatt, M. A. Kovash, H. J. Hausman, T. R. Donoghue, A. D. Bacher, and C. C. Foster, in *Giant Multipole Resonances,* edited by F. E. Bertrand (Harwood, New York, 1980), p. 435; S. L. Blatt, Los Alamos Scientific Laboratory Report No. LA-8303-C, 1980, p. 90.

[10]E. M. Diener, S. L. Blatt, and P. Paul, Nucl. Instrum. Methods 83, 115 (1970).

[11]M. Kovash, Ph.D. dissertation, The Ohio State University, 1978 (unpublished).

[12]H. R. Weller and N. R. Roberson, IEEE Transactions Nucl. Sci. NS-28, 1268 (1981).

[13]A. Nathan, private communication; Evans Hayward and W. Dodge, private communication.

[14]F. Ajzenberg-Selove and C. L. Busch, Nucl. Phys. A336, 60 (1980).

[15]R. E. Marrs, E. G. Adelberger, K. A. Snover, and M. D. Cooper, Phys. Rev. Lett. 35, 202 (1975).

[16]V. Valkovic, D. Milijanic, R. B. Liebert, and G. C. Phillips, Nucl. Phys. A239, 260 (1975).

[17]T. A. Trainor, T. B. Clegg, and P. W. Lisowski, Nucl. Phys. A220, 533 (1974).

[18]C. Rolfs, Nucl. Phys. A217, 29 (1973).

[19]B. Buck and A. A. Pilt, Nucl. Phys. A280, 133 (1977).

[20]A. J. F. Siegert, Phys. Rev. 52, 787 (1937).

[21]J. M. Lafferty, Jr. and S. R. Cotanch, Nucl. Phys. A373, 363 (1982).

[22]G. E. Brown, Nucl. Phys. 57, 339 (1964).

[23]C. M. Vincent and H. T. Fortune, Phys. Rev. C 2, 782 (1970).

[24]R. G. Allas, S. S. Hanna, Luise Meyer-Schutzmeister, and R. E. Segel, Nucl. Phys. 58, 122 (1964).

[25]C. Brassard, H. D. Shay, J. P. Coffin, W. Scholy, and D. A. Bromley, Phys. Rev. C 6, 53 (1971).

[26]J. Noe, P. Paul, K. Snover, M. Suffert, and E. K. Warburton, *International Symposium on Nuclear Structure,* edited by I. Foda-Lovas and G. Palla (Balatonfured, Hungary, 1976).

[27]D. G. Mavis, Ph.d. dissertation, Stanford University, 1977 (unpublished).

[28]K. A. Snover, P. Paul, and H. M. Kuan, Nucl. Phys. A285, 189 (1977).

[29]M. T. Collins, S. Manglos, N. R. Roberson, A. M. Sandorfi, and H. R. Weller, Phys. Rev. C (to be published).

[30]S. Cohen and D. Kurath, Nucl. Phys. A101, 1 (1976).

[31]B. A. Watson, P. P. Singh, and R. E. Segel, Phys. Rev. 182, 977 (1969).

[32]J. R. Calarco, S. W. Wissink, M. Sassao, K. Wienhard, and S. S. Hanna, Phys. Rev. Lett. 39, 925 (1977).

[33]V. Gillet and N. Vinh Mau, Nucl. Phys. 54, 321 (1964).

[34]O. Karban, J. Lowe, P. D. Greaves and V. Hnizdo, Nucl. Phys. A133, 255 (1969).

[35]R. E. Segel, S. S. Hanna, and R. G. Allas, Phys. Rev. 139, 818 (1965). See also E. Salzborn and G. Clausnitzer, in *Polarization Phenomena in Nuclear Reactions,* Proceedings of the Third International Symposium on Polarization in Nuclear Reactions, Madison, Wisconsin, 1970, edited by H. H. Barschall and W. Haeberli (University of Wisconsin, Madison, 1971).

[36]J. T. Londergan and L. D. Ludeking (unpublished).

[37]S. Manglos, N. R. Roberson, H. R. Weller, and D. R. Tilley, Phys. Rev. C 24, 2378 (1981).

[38]M. A. Melkanoff and T. Sawada, Methods Comput. Phys. 6, 1 (1966).

[39]L. Fox and L. T. Goodwin, Proc. Cambridge Philos. Soc. 45, 373 (1949).